Improving Arctic sea-ice thickness estimates with the assimilation of CryoSat-2 summer observations

Chao Min[1], Qinghua Yang[2], Hao Luo[1], Jack Christopher Landy[3], Dake Chen[4], Geoffrey Joseph Dawson[5], Thomas Krumpen[6], Nabir Mamnun[7], Xiaoyu Liu[7], and Lars Nerger[8]

[1]School of Atmospheric Sciences, Sun Yat-sen University, and Southern Marine Science and Engineering Guangdong Laboratory (Zhuhai)
[2]Sun Yat-sen University
[3]University of Tromsø - The Artic University of Norway
[4]State Key Laboratory of Satellite Ocean Environment Dynamics (SOED)
[5]University of Bristol
[6]Alfred Wegener Institute
[7]Alfred Wegener Institute (AWI), Helmholtz Centre for Polar and Marine Research
[8]Alfred Wegener Institute Helmholtz Center for Polar and Marine Research

February 27, 2023

Abstract

Rapidly shrinking Arctic sea ice has had significant impacts on the Arctic Ocean and many outer Arctic regions. It is therefore urgently needed to reliably estimate Arctic sea-ice thickness (SIT) by combined use of available observation and numerical modeling. Here, for the first time, we assimilate the latest CryoSat-2 summer SIT data into a coupled ice-ocean model. In particular, an Incremental Analysis Update scheme is implemented to overcome the discontinuity brought by assimilating biweekly SIT and daily sea ice concentration data. Along with an improvement in sea ice volume, our SIT estimates have smaller errors than that without SIT assimilation in areas where the sea ice is roughest and experiences strong deformation, e.g., around the Fram Strait and Greenland. This study suggests that the newly-developed CryoSat-2 SIT product, when assimilated properly with our approach, has great potential for Arctic sea ice simulation and prediction.

Hosted file

956737_0_art_file_10731458_rqgkpn.docx available at https://authorea.com/users/589030/articles/626059-improving-arctic-sea-ice-thickness-estimates-with-the-assimilation-of-cryosat-2-summer-observations

Hosted file

956737_0_supp_10724632_rqc4nr.docx available at https://authorea.com/users/589030/articles/626059-improving-arctic-sea-ice-thickness-estimates-with-the-assimilation-of-cryosat-2-summer-observations

1

Improving Arctic sea-ice thickness estimates with the assimilation of CryoSat-2 summer observations

Chao Min[1,2], Qinghua Yang[1], Hao Luo[1], Jack C. Landy[3], Dake Chen[1], Geoffrey J. Dawson[4], Thomas Krumpen[2], Nabir Mamnun[2], Xiaoyu Liu[2], and Lars Nerger[2]

[1]School of Atmospheric Sciences, Sun Yat-sen University, and Southern Marine Science and Engineering Guangdong Laboratory (Zhuhai), Zhuhai, China.

[2]Alfred Wegener Institute, Helmholtz Centre for Polar and Marine Research, Bremerhaven, Germany.

[3]Centre for Integrated Remote Sensing and Forecasting for Arctic Operations, Department of Physics and Technology, University of Tromsø The Arctic University of Norway, Tromsø, Norway.

[4]Bristol Glaciology Centre, School of Geographical Sciences, University of Bristol, Bristol, UK.

Corresponding author: Qinghua Yang (yangqh25@mail.sysu.edu.cn)

Key Points:

- CryoSat-2 summer sea-ice thickness (SIT) is assimilated into a coupled ice-ocean model for the first time.

- The discontinuity brought by assimilating biweekly CryoSat-2 SIT is overcome by implementing an incremental analysis update scheme.

- Significant improvements in sea-ice estimates are obtained in the areas where the sea ice is roughest and experiences strong deformation.

Abstract

Rapidly shrinking Arctic sea ice has had significant impacts on the Arctic Ocean and many outer Arctic regions. It is therefore urgently needed to reliably estimate Arctic sea-ice thickness (SIT) by combined use of available observation and numerical modeling. Here, for the first time, we assimilate the latest CryoSat-2 summer SIT data into a coupled ice-ocean model. In particular, an Incremental Analysis Update scheme is implemented to overcome the discontinuity brought by assimilating biweekly SIT and daily sea ice concentration data. Along with an improvement in sea ice volume, our SIT estimates have smaller errors than that without SIT assimilation in areas where the sea ice is roughest and experiences strong deformation, e.g., around the Fram Strait and Greenland. This study suggests that the newly-developed CryoSat-2 SIT product, when assimilated properly with our approach, has great potential for Arctic sea ice simulation and prediction.

Plain Language Summary

In this study, we incorporate the latest biweekly summer sea-ice thickness (SIT) and daily sea-ice concentration (SIC) data from satellite observations into an ice-ocean model to improve the model estimates. Data assimilation (DA) is used here for combining observational data with model simulation. Summer SIT was not assimilated into ice-ocean models before this study. We find better results when we use SIC and summer SIT observations simultaneously with the DA technique than using SIC only. Significant improvements in the SIT field are found in the areas where the sea ice is roughest and experiences strong deformation. This study provides a promising perspective for applying the latest satellite observations of summer SIT to sea ice estimating and forecasting.

1 Introduction

Coinciding with a four-fold Arctic warming ratio compared to the globe on average (Chylek et al., 2022; Rantanen et al., 2022), Arctic sea ice has declined sharply during the satellite era (Kwok, 2018; Stroeve & Notz, 2018). The substantial sea ice loss has significantly influenced the Earth system (Bailey et al., 2021; Cohen et al., 2021; Liu et al., 2022; Qi et al., 2022). For instance, Arctic sea ice reduction is likely linked to extreme events in the middle and lower latitudes (Bailey et al., 2021; Cohen et al., 2021; Liu et al., 2022). Although the ongoing decline has made commercial trans-Arctic transit more feasible in the summer, the changing and

55 mobile sea ice impacts maritime activities (e.g., Eicken, 2013; Min, et al., 2022). For instance,

56 local variations in sea-ice thickness (SIT) can affect the safety and route-planning decisions of

57 maritime navigators. Consequently, there is a great need and interest in reliable measurements,

58 simulations and forecasts of Arctic sea ice.

59   Sophisticated year-round sea-ice concentration (SIC) monitoring has been developed for

60 several decades (e.g., Comiso et al., 1997; Lavergne et al., 2019; Spreen et al., 2008). SIT data

61 like SMOS (Kaleschke et al., 2012; Tian-Kunze et al., 2014), CryoSat-2 (Laxon et al., 2013;

62 Ricker et al., 2014), and ICESat-2 (Kwok et al., 2020; Petty et al., 2020) were enhanced over the

63 year, but have been only available during winter. Recently, a pan-Arctic summer SIT product

64 derived from CryoSat-2 has become available (Landy et al., 2022). The most recent CryoSat-2

65 summer SIT data not only offers the first look at Arctic SIT from the perspective of satellite

66 remote sensing but also unlocks opportunities for constructing a more reliable SIT reanalysis by

67 assimilating this data into dynamical models and generating sea-ice forecasts (Landy et al., 2022).

68   Data assimilation (DA) is highly effective in enhancing sea-ice estimates because the

69 model initialization can be adjusted and the model state can continuously be constrained to

70 reality by integrating new observations (Blockley & Peterson, 2018; Day et al., 2014; Massonnet

71 et al., 2015). The assimilation of winter SIT, for instance, can provide improved initial

72 conditions for the summer season and hence has the potential to lower uncertainty in both sea-ice

73 estimates and forecasts (e.g., Blockley & Peterson, 2018; Day et al., 2014; Mignac et al., 2022;

74 Xie et al., 2018; Yang et al., 2014; Yang et al., 2019). In particular, to improve the ice-thickness

75 estimates, a year-round Combined Model and Satellite Thickness (CMST) reanalysis has been

76 developed by assimilating the CryoSat-2 and SMOS thickness data throughout the freezing

77 season Mu, Losch, et al., 2018). Although CMST has been systematically evaluated and widely

78 used (e.g., Li et al., 2022; Min et al., 2019; Min et al., 2021; Mu, Losch, et al., 2018; Zhou et al.,

79 2021), the SIT is only corrected indirectly in summer through the positive covariance between

80 SIC, which is assimilated, and SIT, which is not during the summer months. Moreover, the

81 weekly mean SIT from CryoSat-2 is simply assimilated every day of the week during the cold

82 season (Mu, Losch, et al., 2018; Mu, Yang, et al., 2018), which may introduce unphysical

83 "jumps" at the transition of different weeks and seasons (i.e., winter-summer and summer-

84 winter). To date, there has not been a study focusing on the impact and approach of assimilating

85 satellite-based summer SIT. Given the current availability of summer SIT data, we conduct a DA

86 experiment by simultaneously assimilating summer SIC and SIT.

87   This study aims to explore whether the assimilation of CryoSat-2 summer SIT data can

88 better constrain modeled SIC and SIT and thus improve sea-ice estimates. We applied an

89 Incremental Analysis Update (IAU) scheme for CryoSat-2 summer SIT assimilation to ensure

90 the physical development of sea-ice volume (SIV) and SIT with CryoSat-2 observations

91 available at a lower biweekly time interval compared to daily SIC observations. We further

92 compare our outputs with CMST and different independent data to assess the overall

93 improvement by assimilating summer SIT.

2 Materials and Methods

94

2.1 Satellite-retrieved observations

95

96   The pan-Arctic year-round CryoSat-2 SIT dataset has been generated by combining deep

97 learning radar waveform classification with numerical radar simulations (Landy et al., 2022). In

98 summary, a one-dimensional convolutional neural network (CNN) has been applied to classify

99 leads from sea-ice returns in radar altimeter waveforms (Dawson et al., 2022). A series of

100 numerical waveform simulations based on the Facet-Based Echo Model (Landy et al., 2020;

101 Landy et al., 2019), which integrates melt ponds, are then used to calibrate a radar range bias that

102 causes the CryoSat-2 freeboards to be underestimated. The SIT is derived from CryoSat-2 radar

103 freeboards assuming hydrostatic equilibrium and accounting for snow loading, with snow depth

104 and density estimates obtained from SnowModel-LG (https://nsidc.org/data/nsidc-

105 0758/versions/1; Stroeve et al., 2020). The innovative dataset provides SIT and its uncertainty

106 with a temporal resolution of 15 or 16 days and a spatial resolution of 80 km. Large uncertainties

107 still remain, nevertheless, close to the coast of northern Greenland and the Fram Strait when

108 compared to airborne electromagnetic (AEM) thickness observations (Landy et al., 2022). More

109 details about data processing can be found in Dawson et al. (2022) and Landy et al. (2022).

110   The SIC data used in this study is computed at the French Research Institute for

111 Exploitation of the Sea (IFREMER) and reprocessed by the Integrated Climate Data Center.

112 Together with the ARTIST Sea Ice algorithm (Kaleschke et al., 2001; Spreen et al., 2008), this

113 SIC dataset is derived from brightness temperatures measured with the 85-GHz Special Sensor

114 Microwave / Imager (SSM/I) and/or Special Sensor Microwave / Imager Sounder (SSM/IS)

115   channels. A 5-day median filter is used to reduce unrealistic short-term SIC variations resulting

116   from weather influence (Kern et al., 2010). The spatial resolution of the daily SIC data is 12.5

117   km.

118   **2.2 Reference observations**

119   The sea-ice extents (SIEs) estimated from CMST and our experiments are evaluated

120   using the SIC observation that is processed by the NASA team algorithm and distributed by

121   National Snow and Ice Data Center (NSIDC, DiGirolamo et al., 2022). This independent SIC

122   dataset is used to ensure we are not assimilating and testing against the same observations.

123   Moreover, to validate the SIT results, we use a set of independent fixed mooring and airborne sea

124   ice thickness observations (see Fig. 1 for geographic locations of surveys and deployment

125   positions). Sea ice drafts were obtained from upward-looking sonars (ULS) provided by the

126   Beaufort Gyre Experiment Program (BGEP) in 2015. Data from three different moorings are

127   hereafter referred to as BGEP_A, BGEP_B and BGEP_D. According to Melling et al. (1995),

128   the error associated with ULS sea ice draft observations is about 0.1 m. In addition, we used draft

129   data based on an Acoustic Doppler Current Profiler (ADCP) deployed by the Alfred Wegener

130   Institute (AWI) in the western Laptev Sea area in 2014. Following Belter et al. (2021), the

131   uncertainties are relatively high (±0.96 m) but consistent. To simplify the comparison between

132   model SIT and observations, the observed sea ice draft is converted to thickness by multiplying

133   by a factor of 1.1 (Nguyen et al., 2011).

134   In addition to the moored observations, SIT from airborne electromagnetic (AEM)

135   surveys (IceBird campaign) conducted by AWI in Fram Strait and northern Greenland (Krumpen

136   et al., 2019) are used as a reference dataset for our model results. The applied surveys were

137   conducted between 24 July and 1 August 2016 during the IceBird campaign. For more details on

138   the methodology, we refer to Krumpen et al. (2020). According to Pfaffling et al. (2007), AEM

139   observations are estimated to have an uncertainty of ±0.1 m over flat ice, although the accuracy

140   may be affected by the presence of melt ponds. As the footprint of airborne measurements is in

141   the range of tens of meters, all AEM-based SIT are averaged onto the CroSat-2 grids for

142   comparison, following Landy et al. (2022). As the numerical model carries the effective/mean

143   ice thickness (volume over an area), all field observations are multiplied by the local NSIDC SIC

144   to obtain the observed mean thickness to facilitate the comparison between the model and

145   observations following Yang et al. (2015).

146   **2.3 Sea-ice data assimilation system**

147   The DA system is further developed based on the CMST system. I.e., the Massachusetts

148   Institute of Technology general circulation model (MITgcm, Marshall et al., 1997) and the

149   Parallel Data Assimilation Framework (PDAF, Nerger & Hiller, 2013) are employed. The sea ice

150   dynamics use a viscous plastic rheology (Hibler, 1979; Zhang & Hibler, 1997), with a one-layer,

151   zero-heat capacity formulation applied in the thermodynamics (Parkinson & Washington, 1979;

152   Semtner, 1976). 50 vertical model layers are used in the ocean model, with 28 layers located in

153   the top 1000 m. An Arakawa C grid with a variable horizontal resolution with an average

154   spacing of 18 km, is used to discretize both the ocean and sea ice models. The experiments are

155   based on a regional MITgcm configuration with open boundaries located around 55°N in the

156   Atlantic and Pacific (Losch et al., 2010; Nguyen et al., 2011). Figure 1 depicts the model domain

157   with an orange mesh.

158   As with earlier DA studies (e.g., Mu, Losch, et al., 2018; Mu, Yang, et al., 2018; Yang et

159   al., 2015), the coupled ice-ocean model is driven by atmospheric ensemble forecasts generated

160   by the UK Met Office (UKMO) Ensemble Prediction System (EPS) and accessible from the

161   THORPEX Interactive Grand Global Ensemble archive (TIGGE) (Bowler et al., 2008; Park et al.,

162   2008) in order to incorporate flow-dependent uncertainty in atmospheric forcing. Eleven sets of

163   perturbed forecasts are employed to force an ensemble of eleven model states. Details about

164   atmospheric data processing can be found in previous works (Mu, Losch, et al., 2018; Yang et

165   al., 2015).

166   For easy comparison with the previously developed CMST reanalysis, which only

167   assimilates IFREMER SIC during summer, following Mu et al. (2018), the IFREMER SIC and

168   CryoSat-2 SIT are assimilated into the ice-ocean model by using the local error-subspace

169   transform Kalman filter (LESTKF) coded in PDAF (Nerger & Hiller, 2013; Nerger et al., 2012).

170   The LESTKF is a highly efficient ensemble Kalman filter with very high-dimensional models

171   (Nerger et al., 2012). SIC and SIT obtained from the forecast fields are stored together in the

172   state vector. Then, in each analysis step, the LESTKF is used to correct the state vector by only

173   taking into account the sea-ice data observed within a 126 km radius of each model point (Mu,

174 Losch, et al., 2018; Yang et al., 2015). The observations within the radius are weighted with

175 distance from the grid point by a quasi-Gaussian weight function (Gaspari & Cohn, 1999).

176 Model uncertainties are calculated from the ensemble of model states driven by the UKMO

177 ensemble atmospheric forcing (Mu, Losch, et al., 2018; Yang et al., 2015). The observation error

178 for SIC is set as a constant value of 0.25, while the variable SIT observation errors are provided

179 by the CryoSat-2 dataset (Mu, Losch, et al., 2018; Yang et al., 2015).

180   For consistent pan-Arctic temporal and spatial coverage, the CryoSat-2 SIT data is

181 available twice per month at an interval of 15 or 16 days (Landy et al., 2022; Lawrence et al.,

182 2021). Therefore, the forecast interval between the analysis steps will be excessively long when

183 assimilating CryoSat-2 data directly. The sparse analysis step typically creates unrealistically

184 large "jumps" (increments) for the evolution of sea ice, leading to an unnatural development of

185 SIV (figures are not shown). For forecasting systems that need daily updates, direct assimilation

186 of this data is therefore inappropriate. Hence, an IAU strategy similar to previous studies (Bloom

187 et al., 1996; Lellouche et al., 2013; Ourmières et al., 2006) is implemented to obtain smoother

188 evolutions of sea ice. In brief, we run a 7-/8-day experiment that assimilates daily SIC and, when

189 available, biweekly CryoSat-2 SIT. The SIT increment obtained at the analysis step that both SIC

190 and SIT are assimilated is not applied immediately, but divided by each biweekly CryoSat-2's

191 number of days, and stored for the IAU to make daily updates. Finally, the DA system is

192 restarted assimilating daily SIC and incorporating daily SIT increments and producing the

193 analysis fields. This approach allows us to assimilate the rather infrequent biweekly summer SIT

194 data in combination with the daily SIC data, while ensuring a gradual development of the sea ice

195 fields over time. A detailed description of the IAU scheme developed in this study is provided in

196 Text S1 and Figure S1 in Supporting Information S1.

197   **2.4 Experiment design**

198   The beginning of 2016 experienced record-low monthly SIE but the summer extent

199 exceeded most seasonal forecasts (Petty et al., 2017; Petty et al., 2018). Due to the

200 unconsolidated summer ice cover in 2016, modeling and forecasting sea ice conditions during

201 this summer are expected to be exceptionally challenging (Petty et al., 2017; Petty et al., 2018).

202 Therefore, we carried out the DA experiment from May 23 to September 30, 2016. The

203 performance of our experiments during the year 2016 is, therefore, a performance assessment

204   indicator of this system. Given that CMST data is already well-validated and applied (e.g., Li et

205   al., 2022; Min et al., 2019; Min et al., 2021; Mu, Losch, et al., 2018; Zhou et al., 2021),

206   following Yang et al (2019), restart files from this retrospective simulation (CMST) were used as

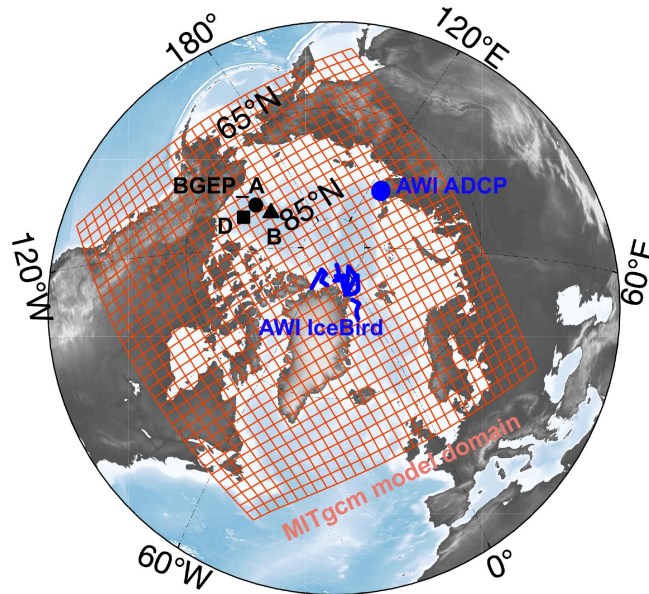207   the initial ice-ocean conditions for the DA experiments.

208

209   **Figure 1**. The MITgcm model grid is shown in an orange net plotted at every 12 model grid

210   points. The independent observations used to validate CryoSat-2, Combined Model and Satellite

211   Thickness (CMST) and the analysis field (ANA) are presented in blue extra-large dots for two

212   AWI Acoustic Doppler Current Profiler (ADCP) sensor deployments, in blue lines for the AWI

213   airborne surveys (IceBird), and in black dot, triangle and square for Beaufort Gyre Exploration

214   Program (BGEP) moorings A, B and D, respectively. The blue dots for two AWI ADCPs (Vilk1-

215   14 and Vilk3-14) are overlapped because of their near proximity.

216   **3 Results**

217   The spatial distributions of summer SIT are displayed in Figures 2a-2c and the daily

218   evolution of SIE in Figure 2d and SIV in Figure 2e. Overall, the assimilation of summer SIT

219   leads to a better agreement of the SIT and SIV estimated from our thickness analysis field

220   (hereafter, ANA) with that from CryoSat-2 compared to CMST, which only assimilates SIC

221   during the summer. Compared to CMST, the additional assimilation of summer SIT leads to an

222   SIT distribution that is more similar to that from CryoSat-2 (Figures 2a-2c). The overestimation

223   of the ice thickness by CMST is corrected particularly in the Fram Strait and in the Arctic Ocean

224   on the northern coast of the Canadian Arctic Archipelago and Greenland. These are regions

225   where the sea ice experiences strong deformation and the ice surface is roughest (Farrell et al.,

226   2020; Kwok, 2015). Further, our results demonstrate relatively strong agreement with observed

227   SIE and SIV during the entire summer season (Figures 2d-2e), both during the ice melting phase

228   and freezing timing (mid-September).

229   Root-mean-square error (RMSE), mean bias (MB), and correlation coefficient (CC),

230   whose calculation methods are described in Text S2 in Supporting Information S1, are used to

231   quantify comparisons between CMST, ANA, and observations. The CCs for SIE and SIV

232   between ANA/CMST and observations are nearly equal. Statistically, the CC for SIE between

233   ANA and NSIDC data is ~1, while for SIV, it is 0.97 between ANA and CryoSat-2 data. The

234   RMSE for SIE calculated from ANA and observations is roughly 0.72×10^6 km^2, although it is

235   somewhat bigger when calculated using CMST and observations, where it is 0.74×10^6 km^2. In

236   relation to the SIV calculated by CMST and ANA, the RMSEs are likewise decreased from

237   2.43×10^3 km^3 to 1.97×10^3 km^3, demonstrating that the further assimilation of summer SIT

238   improves the estimates for both SIE and SIV. We notice that the initial state from CMST still

239   exhibits a large error in estimating SIV even though it has assimilated SIT and SIC throughout

240   the cold season and assimilated SIC during the summer season. Besides, we hypothesize that

241   there are two reasons why there is still a significant misfit between ANA and CryoSat-2 until the

242   end of June. First, the DA system takes a certain period to spin up itself before leading to

243   consistent improvements (Mu, Yang, et al., 2018). Second, around the end of May and June,

244   CryoSat-2 exhibits substantially higher uncertainty than the model state, bringing our ANA
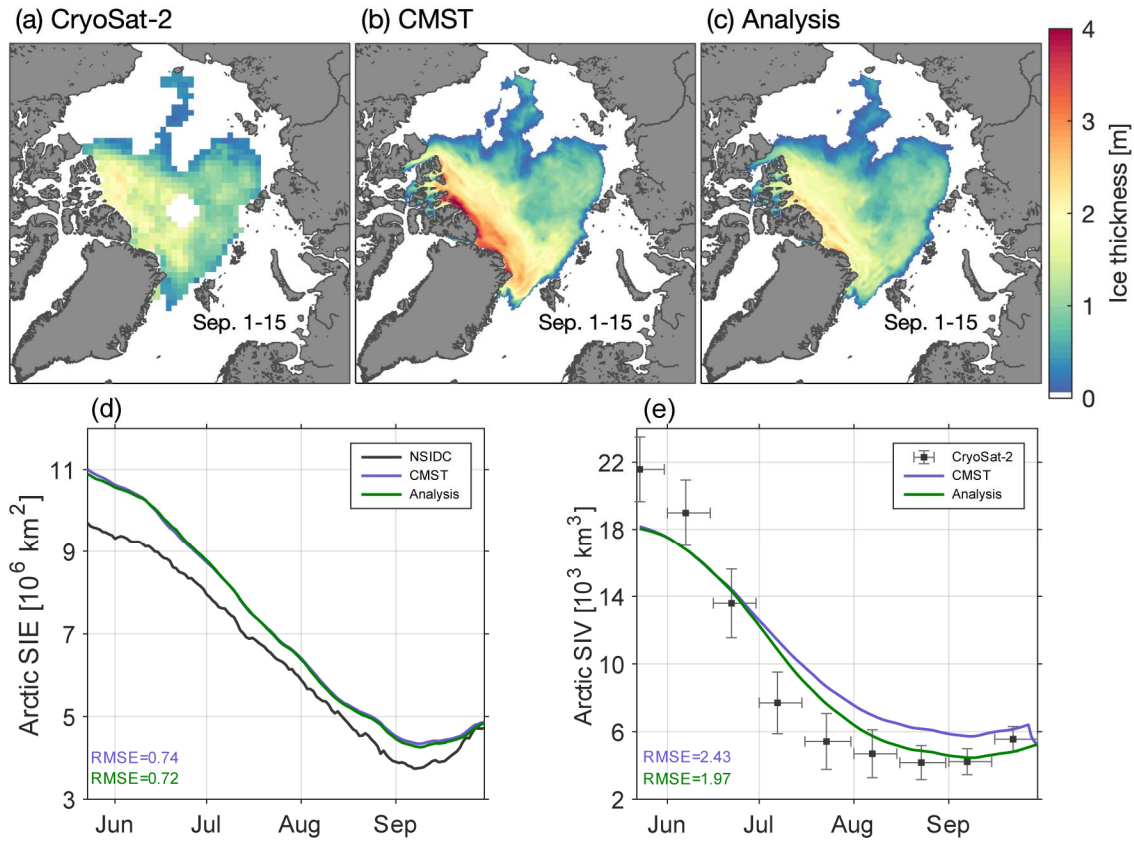
245   closer to the model state.

Figure 2. Arctic sea-ice thickness averaged over September 1-15, 2016 from CryoSat-2, Combined Model and Satellite Thickness (CMST) and Analysis (ANA) are shown in (a), (b) and (c). Panels (d) and (e) present the developments of summer sea-ice extent (SIE) and volume (SIV), respectively. The vertical bar in (e) for CryoSat-2 is for uncertainty and the horizontal bar is the time span for biweekly CryoSat-2 data. Root-mean-square errors (RMSEs) shown in purple and green are for CMST against observations and ANA against observations, respectively.

Because the sea-ice model's parameterizations are imperfect and satellite measurements of ice thickness have significant uncertainties in coastal areas of thick MYI, the CMST analysis is most uncertain around the northern coast of the Canadian Arctic Archipelago and Greenland (Mu, Losch, et al., 2018). Comparisons between ANA, CMST, CryoSat-2, and airborne sea ice surveys (Figure 3) are conducted to determine differences in certain places where strong sea-ice deformation occurs. As shown in Figure 2b, CMST appears to estimate excessively thick ice in these regions, whereas CryoSat-2 measures thinner sea ice than airborne surveys, as shown in

261   Landy et al. (2022). The median values of airborne surveys, CMST and CryoSat-2 are 1.58 m,

262   2.33 m and 0.9 m, respectively. With a median of 1.86 m, which is closest to that of the airborne

263   surveys, ANA has the best agreement among CryoSat-2, CMST, and ANA. This likewise holds

264   for the dominating probability density estimates for the observed and simulated SIT. The best

265   agreement between airborne surveys and ANA is also verified by their lower and upper quartiles.

266   Benefiting from the model dynamics and summer SIT assimilation, our ANA has reduced the

267   overestimation of ice thickness in CMST, particularly in the Arctic coasts of north Greenland,

268   while preventing the underestimation evident in CryoSat-2 observations.

269
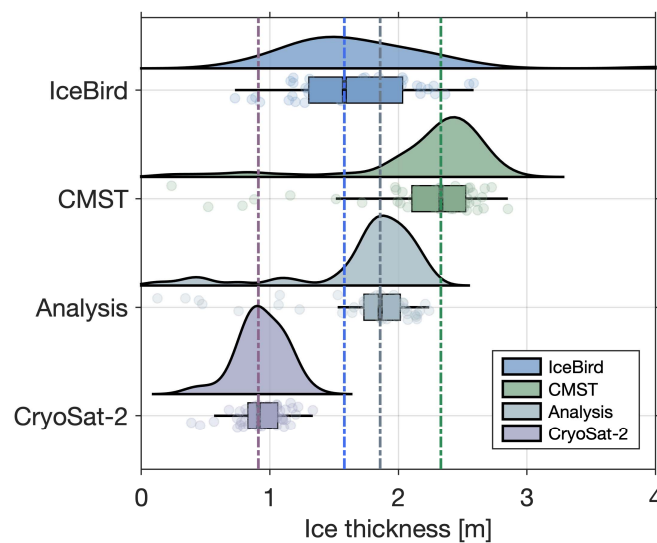
Figure 3. Comparison between observed sea-ice thickness (SIT) from the airborne surveys

271   (IceBird) and CryoSat-2, simulated SIT from the Combined Model and Satellite Thickness

272   (CMST) and Analysis (ANA). The raincloud plots show the distributions of observed and

273   simulated SIT and their key summary statistics (i.e., lower and upper quartiles, medians, and

274   outliers). The medians for IceBird observations, CMST, ANA and CryoSat-2 are represented by

275   blue, green, gray and violet dashed lines, respectively. Translucent dots represent the observed

276   and simulated SIT exactly.

277   With sea-ice observations from BGEP moorings, the performance of CryoSat-2, CMST

278   and ANA are assessed in the Beaufort Sea (Figure 4, Tables 1 and Table S1 in Supporting

279   Information S1). The three datasets replicate the SIT developments that were measured by in-situ

280   measurements (Figures 4a-4c). Compared to BGEP moorings, both CMST and ANA show

281   comparatively small RMSE and MB. For the BGEP measurements, the RMSEs for ANA are up

282 to 0.05 m smaller than for CMST, while the MB is generally below 0.10 m and differs by up to

283 0.06 m, indicating that the further assimilation of CryoSat-2 improves not only the estimate of

284 Arctic SIV but also the local SIT. It should be noted that the growth in SIT at the location of

285 BGEP_B during mid- to late-September (Fig. 4b) is only well captured by ANA, which

286 integrates model dynamics with satellite SIT.

287 Compared to AWI ADCPs (i.e., Vilk1-14 and Vilk3-14) deployed in the Laptev Sea,

288 CryoSat-2, CMST and ANA have relatively larger deviations (Figures 4d-4e). The RMSEs for

289 ANA versus Vilk1-14 and Vilk3-14 are 0.61 m and 0.78 m while the MBs are –0.39 m and –0.43

290 m. Although the SIT as measured by AWI ADCPs is underestimated by our model outputs, the

291 MB for ANA is within the AWI ADCPs' uncertainty (±0.96 m). Further, the CryoSat-2 data

292 shows an even larger underestimation. However, in contrast to the BGEP time series, the

293 evolution of the SIT at the Vilk moorings was complex during summer 2016. The ice cover

294 actually thickened between the start and end of the summer as highly-deformed ice was

295 transiting the mooring locations (Belter et al., 2020). This demonstrates that ANA still functions

296 in the Laptev Sea. Since the Laptev Sea is a crucial sea area affecting navigation safety (e.g.,

297 Min et al., 2022; Min et al., 2023), both observations and model simulations need to be further

298 optimized for sea ice conditions in unusual years like 2016.

299 **Table 1**. Main statistics [m] used to verify the sea-ice thickness of the Combined Model and

300 Satellite Thickness (CMST) and Analysis (ANA) against in-situ measurements (i.e., BGEP_A,

301 BGEP_B, BGEP_D, Vilk1-14 and Vilk3-14) over the summer period in 2016.

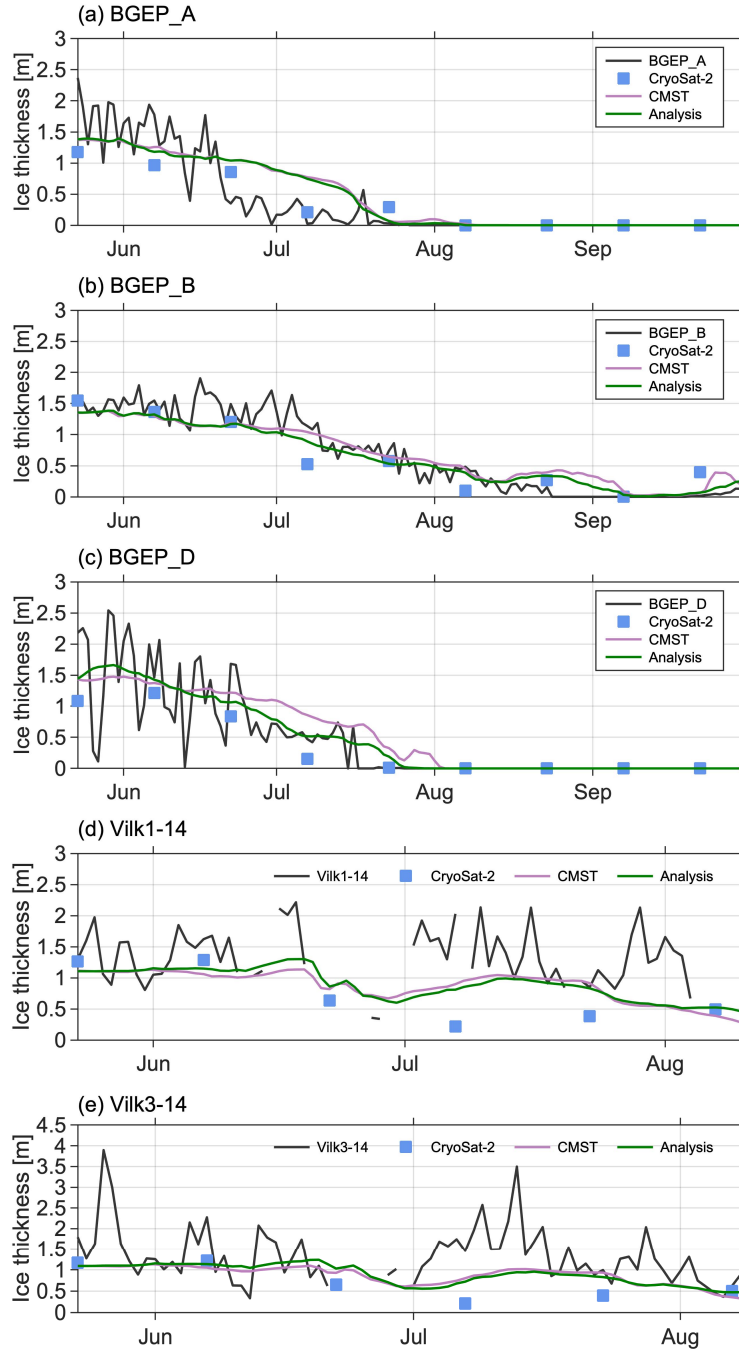| In-situ observation	RMSE		MB	
	CMST	ANA	CMST	ANA
BGEP_A	0.35	0.35	0.08	0.07
BGEP_B	0.24	0.23	0.01	−0.05
BGEP_D	0.40	0.35	0.09	0.03
Vilk1-14	0.61	0.61	−0.40	−0.39
Vilk3-14	0.76	0.78	−0.45	−0.43

302

Figure 4. Comparison of summer sea-ice thickness (SIT) from the Beaufort Gyre Exploration Program (BGEP) moorings, CryoSat-2, Combined Model and Satellite Thickness (CMST) and Analysis (ANA), during summer 2016. (a, b and c) are for SIT developments at BGEP_A, BGEP_B and BGEP_D. Panels (d) and (e) are for SIT developments at AWI Acoustic Doppler Current Profiler (ADCP) sensor deployments (Vilk1-14 and Vilk3-14) in the Laptev Sea.

4 Conclusions and discussions

To investigate the impact of assimilating the recent CryoSat-2 summer SIT in estimating Arctic summer SIT, we have carried out a DA experiment including a novel IAU approach. This method guarantees a gradual development of the sea-ice fields over time while allowing the assimilation of the infrequent summer SIT data, which is only provided on a two-week basis, in conjunction with the daily SIC data. The model dynamics play an important role in the assimilation and have the potential to reduce the underestimation of SIT in satellite retrievals, especially along the Arctic coasts of Greenland (Landy et al., 2022), where the ice thermodynamically thickens as well as experiences deformation over many winter seasons (Kwok, 2015; Tschudi et al., 2016). Likewise, our ANA basically solves the overestimation of SIT estimated by CMST in those areas and thus provides a more reliable estimate of summer SIT. Moreover, in comparison to the CMST reanalysis, which did not assimilate this summer SIT data, the evolution of the SIV estimates agrees better with that derived from CryoSat-2.

These findings demonstrate the benefits of assimilating CryoSat-2 summer SIT for estimating Arctic sea ice and hence improving the initial states for sea-ice forecasts. As a result, the sea-ice forecast, which is highly relevant for marine activities, can benefit greatly from the enhanced initial states (Xiu et al., 2022; Yang et al., 2019). Further, our IAU assimilation scheme can be well applied to summer sea ice assimilation, which is important for developing a sea-ice reanalysis that assimilates year-round satellite ice thickness and concentration. A continuous long-term ice thickness record with a finer temporal-spatial resolution that assimilates both year-round SIC and SIT will be reconstructed in the future.

Acknowledgments

347 **Open Research**

348 All data used in this study are openly accessible. The BGEP ULS-measured sea-ice draft data
349 were downloaded from https://www2.whoi.edu/site/beaufortgyre/data/mooring-data/. The sea-ice
350 draft data measured by AWI ADCP sensors were downloaded from
351 https://doi.pangaea.de/10.1594/PANGAEA.912927. The SIC data provided by the National
352 Snow and Ice Data Center and the University of Hamburg are available at
353 https://nsidc.org/data/nsidc-0051/versions/2 and https://www.cen.uni-hamburg.de/en/icdc/data/,
354 respectively. The UKMO ensemble forecasting data were obtained from the THORPEX
355 Interactive Grand Global Ensemble (TIGGE) archive
356 (https://apps.ecmwf.int/datasets/data/tigge/levtype=sfc/type=cf/). The CryoSat-2 SIT data is
357 available from the British Antarctic Survey Polar Data Centre at
358 https://doi.org/10.5285/D8C66670-57AD-44FC-8FEF-942A46734ECB. The MITgcm model
359 code is available at http://mitgcm.org. PDAF can be obtained from http://pdaf.awi.de.

360

361 **References**

362 Bailey, H., Hubbard, A., Klein, E. S., Mustonen, K.-R., Akers, P. D., Marttila, H., & Welker, J.
363   M. (2021). Arctic sea-ice loss fuels extreme European snowfall. *Nature Geoscience,*
364   *14*(5), 283-288. https://doi.org/10.1038/s41561-021-00719-y
365 Belter, H. J., Krumpen, T., Hendricks, S., Hoelemann, J., Janout, M. A., Ricker, R., & Haas, C.
366   (2020). Satellite-based sea ice thickness changes in the Laptev Sea from 2002 to 2017:
367   comparison to mooring observations. *The Cryosphere, 14*(7), 2189-2203.
368   https://doi.org/10.5194/tc-14-2189-2020

Belter, H. J., Krumpen, T., Janout, M. A., Ross, E., & Haas, C. (2021). An Adaptive Approach to Derive Sea Ice Draft from Upward-Looking Acoustic Doppler Current Profilers (ADCPs), Validated by Upward-Looking Sonar (ULS) Data. *Remote Sensing, 13*(21). https://doi.org/10.3390/rs13214335

Blockley, E. W., & Peterson, K. A. (2018). Improving Met Office seasonal predictions of Arctic sea ice using assimilation of CryoSat-2 thickness. *The Cryosphere, 12*(11), 3419-3438. https://doi.org/10.5194/tc-12-3419-2018

Bloom, S. C., Takacs, L. L., da Silva, A. M., & Ledvina, D. (1996). Data Assimilation Using Incremental Analysis Updates. *Monthly Weather Review, 124*(6), 1256-1271. https://doi.org/10.1175/1520-0493(1996)124<1256:DAUIAU>2.0.CO;2

Bowler, N. E., Arribas, A., Mylne, K. R., Robertson, K. B., & Beare, S. E. (2008). The MOGREPS short-range ensemble prediction system. *Quarterly Journal of the Royal Meteorological Society, 134*(632), 703-722. https://doi.org/10.1002/qj.234

Chylek, P., Folland, C., Klett, J. D., Wang, M., Hengartner, N., Lesins, G., & Dubey, M. K. (2022). Annual Mean Arctic Amplification 1970–2020: Observed and Simulated by CMIP6 Climate Models. *Geophysical Research Letters, 49*(13), e2022GL099371. https://doi.org/10.1029/2022GL099371

Cohen, J., Agel, L., Barlow, M., Garfinkel, C. I., & White, I. (2021). Linking Arctic variability and change with extreme winter weather in the United States. *Science, 373*(6559), 1116-1121. https://doi.org/10.1126/science.abi9167

Comiso, J. C., Cavalieri, D. J., Parkinson, C. L., & Gloersen, P. (1997). Passive microwave algorithms for sea ice concentration: A comparison of two techniques. *Remote Sensing of Environment, 60*(3), 357-384. https://doi.org/10.1016/S0034-4257(96)00220-9

Dawson, G., Landy, J., Tsamados, M., Komarov, A. S., Howell, S., Heorton, H., & Krumpen, T. (2022). A 10-year record of Arctic summer sea ice freeboard from CryoSat-2. *Remote Sensing of Environment, 268*, 112744. https://doi.org/10.1016/j.rse.2021.112744

Day, J. J., Hawkins, E., & Tietsche, S. (2014). Will Arctic sea ice thickness initialization improve seasonal forecast skill? *Geophysical Research Letters, 41*(21), 7566-7575. https://doi.org/10.1002/2014GL061694

398 DiGirolamo, N., Parkinson, C. L., Cavalieri, D. J., Gloersen, P., & Zwally, H. J. (2022). Sea Ice
399   Concentrations from Nimbus-7 SMMR and DMSP SSM/I-SSMIS Passive Microwave
400   Data*, Version 2 [Data Set],* https://doi.org/10.5067/MPYG15WAA4WX.
401 Eicken, H. (2013). Arctic sea ice needs better forecasts. *Nature, 497*(7450), 431-433.
402   https://doi.org/10.1038/497431a
403 Farrell, S. L., Duncan, K., Buckley, E. M., Richter-Menge, J., & Li, R. (2020). Mapping Sea Ice
404   Surface Topography in High Fidelity With ICESat-2. *Geophysical Research Letters,*
405   *47*(21), e2020GL090708. https://doi.org/10.1029/2020GL090708
406 Gaspari, G., & Cohn, S. E. (1999). Construction of correlation functions in two and three
407   dimensions. *Quarterly Journal of the Royal Meteorological Society, 125*(554), 723-757.
408   https://doi.org/10.1002/qj.49712555417
409 Hibler, W. D. (1979). A Dynamic Thermodynamic Sea Ice Model. *Journal of Physical*
410   *Oceanography,   9*(4),   815-846.   https://doi.org/10.1175/1520-
411   0485(1979)009<0815:ADTSIM>2.0.CO;2
412 Kaleschke, L., Tian-Kunze, X., Maaß, N., Mäkynen, M., & Drusch, M. (2012). Sea ice thickness
413   retrieval from SMOS brightness temperatures during the Arctic freeze-up period.
414   *Geophysical Research Letters, 39*(5). https://doi.org/10.1029/2012GL050916
415 Kaleschke, L., Lupkes, C., Vihma, T., Haarpaintner, J., Bochert, A., Hartmann, J., & Heygster,
416   G. (2001). SSM/I sea ice remote sensing for mesoscale ocean-atmosphere interaction
417   analysis. *Canadian   Journal   of   Remote   Sensing,   27*(5),   526-537.
418   https://doi.org/10.1080/07038992.2001.10854892
419 Kern, S., Kaleschke, L., & Spreen, G. (2010). Climatology of the Nordic (Irminger, Greenland,
420   Barents, Kara and White/Pechora) Seas ice cover based on 85 GHz satellite microwave
421   radiometry: 1992–2008. *Tellus A: Dynamic Meteorology and Oceanography, 62*(4), 411-
422   434. http://doi.org/10.1111/j.1600-0870.2009.00457.x
423 Krumpen, T., Belter, H. J., Boetius, A., Damm, E., Haas, C., Hendricks, S., et al. (2019). Arctic
424   warming interrupts the Transpolar Drift and affects long-range transport of sea ice and
425   ice-rafted matter. Scientific Reports, 9(1), 5459. https://doi.org/10.1038/s41598-019-
426   41456-y

427 Krumpen, T., Birrien, F., Kauker, F., Rackow, T., von Albedyll, L., Angelopoulos, M., et al.
428   (2020). The MOSAiC ice floe: sediment-laden survivor from the Siberian shelf. The
429   Cryosphere, 14(7), 2173-2187. https://doi.org/10.5194/tc-14-2173-2020

430 Kwok, R. (2015). Sea ice convergence along the Arctic coasts of Greenland and the Canadian
431   Arctic Archipelago: Variability and extremes (1992–2014). *Geophysical Research*
432   *Letters, 42*(18), 7598-7605. https://doi.org/10.1002/2015GL065462

433 Kwok, R. (2018). Arctic sea ice thickness, volume, and multiyear ice coverage: losses and
434   coupled variability (1958–2018). *Environmental Research Letters, 13*(10), 105005.
435   https://doi.org/10.1088/1748-9326/aae3ec

436 Kwok, R., Kacimi, S., Webster, M. A., Kurtz, N. T., & Petty, A. A. (2020). Arctic Snow Depth
437   and Sea Ice Thickness From ICESat-2 and CryoSat-2 Freeboards: A First Examination.
438   *Journal of Geophysical Research: Oceans, 125*(3), e2019JC016008.
439   https://doi.org/10.1029/2019JC016008

440 Landy, J. C., Tsamados, M., & Scharien, R. K. (2019). A Facet-Based Numerical Model for
441   Simulating SAR Altimeter Echoes From Heterogeneous Sea Ice Surfaces. *IEEE*
442   *Transactions on Geoscience and Remote Sensing, 57*(7), 4164-4180.
443   https://doi.org/10.1029/2008JC004753

444 Landy, J. C., Petty, A. A., Tsamados, M., & Stroeve, J. C. (2020). Sea Ice Roughness
445   Overlooked as a Key Source of Uncertainty in CryoSat-2 Ice Freeboard Retrievals.
446   *Journal of Geophysical Research: Oceans, 125*(5), e2019JC015820.
447   https://doi.org/10.1029/2019JC015820

448 Landy, J. C., Dawson, G. J., Tsamados, M., Bushuk, M., Stroeve, J. C., Howell, S. E. L., et al.
449   (2022). A year-round satellite sea-ice thickness record from CryoSat-2. *Nature*.
450   https://doi.org/10.1038/s41586-022-05058-5

451 Lavergne, T., Sørensen, A. M., Kern, S., Tonboe, R., Notz, D., Aaboe, S., et al. (2019). Version
452   2 of the EUMETSAT OSI SAF and ESA CCI sea-ice concentration climate data records.
453   *The Cryosphere, 13*(1), 49-78. https://doi.org/10.5194/tc-13-49-2019

454 Lawrence, I. R., Armitage, T. W. K., Tsamados, M. C., Stroeve, J. C., Dinardo, S., Ridout, A. L.,
455   et al. (2021). Extending the Arctic sea ice freeboard and sea level record with the
456   Sentinel-3 radar altimeters. *Advances in Space Research, 68*(2), 711-723.
457   https://doi.org/10.1016/j.asr.2019.10.011

458 Laxon, S. W., Giles, K. A., Ridout, A. L., Wingham, D. J., Willatt, R., Cullen, R., et al. (2013).
459   CryoSat-2 estimates of Arctic sea ice thickness and volume. *Geophysical Research*
460   *Letters, 40*(4), 732-737. https://doi.org/10.1002/grl.50193

461 Lellouche, J. M., Le Galloudec, O., Drévillon, M., Régnier, C., Greiner, E., Garric, G., et al.
462   (2013). Evaluation of global monitoring and forecasting systems at Mercator Océan.
463   *Ocean Sci., 9*(1), 57-81. https://doi.org/10.5194/os-9-57-2013

464 Li, X., Yang, Q., Yu, L., Holland, P. R., Min, C., Mu, L., & Chen, D. (2022). Unprecedented
465   Arctic sea ice thickness loss and multiyear-ice volume export through Fram Strait during
466   2010–2011. *Environmental Research Letters, 17*(9), 095008.
467   https://doi.org/10.1088/1748-9326/ac8be7

468 Liu, J., Song, M., Zhu, Z., Horton, R. M., Hu, Y., & Xie, S.-P. (2022). Arctic sea-ice loss is
469   projected to lead to more frequent strong El Niño events. *Nature Communications, 13*(1),
470   4952. https://doi.org/10.1038/s41467-022-32705-2

471 Losch, M., Menemenlis, D., Campin, J.-M., Heimbach, P., & Hill, C. (2010). On the formulation
472   of sea-ice models. Part 1: Effects of different solver implementations and
473   parameterizations. *Ocean Modelling, 33*(1), 129-144.
474   https://doi.org/10.1016/j.ocemod.2009.12.008

475 Marshall, J., Adcroft, A., Hill, C., Perelman, L., & Heisey, C. (1997). A finite-volume,
476   incompressible Navier Stokes model for studies of the ocean on parallel computers.
477   *Journal of Geophysical Research: Oceans, 102*(C3), 5753-5766.
478   https://doi.org/10.1029/96JC02775

479 Massonnet, F., Fichefet, T., & Goosse, H. (2015). Prospects for improved seasonal Arctic sea ice
480   predictions from multivariate data assimilation. *Ocean Modelling, 88*, 16-25.
481   https://doi.org/10.1016/j.ocemod.2014.12.013

482 Melling, H., Johnston, P. H., & Riedel, D. A. (1995). Measurements of the Underside
483   Topography of Sea-Ice by Moored Subsea Sonar. *Journal of Atmospheric and Oceanic*
484   *Technology, 12*(3), 589-602. https://doi.org/10.1175/1520-
485   0426(1995)012<0589:MOTUTO>2.0.CO;2

486 Mignac, D., Martin, M., Fiedler, E., Blockley, E., & Fournier, N. (2022). Improving the Met
487   Office's Forecast Ocean Assimilation Model (FOAM) with the assimilation of satellite-
488   derived sea-ice thickness data from CryoSat-2 and SMOS in the Arctic. *Quarterly*

489   *Journal of the Royal Meteorological Society, 148*(744), 1144-1167.
490   https://doi.org/10.1002/qj.4252

491   Min, C., Mu, L., Yang, Q., Ricker, R., Shi, Q., Han, B., et al. (2019). Sea ice export through the
492   Fram Strait derived from a combined model and satellite data set. *The Cryosphere,*
493   *13*(12), 3209-3224. https://doi.org/10.5194/tc-13-3209-2019

494   Min, C., Yang, Q., Mu, L., Kauker, F., & Ricker, R. (2021). Ensemble-based estimation of sea-
495   ice volume variations in the Baffin Bay. *The Cryosphere, 15*(1), 169-181.
496   https://doi.org/10.5194/tc-15-169-2021

497   Min, C., Yang, Q., Chen, D., Yang, Y., Zhou, X., Shu, Q., & Liu, J. (2022). The Emerging
498   Arctic Shipping Corridors. *Geophysical Research Letters, 49*(10), e2022GL099157.
499   https://doi.org/10.1029/2022GL099157

500   Min, C., Zhou, X., Luo, H., Yang, Y., Wang, Y., Zhang, J., & Yang, Q. (2023). Toward
501   Quantifying the Increasing Accessibility of the Arctic Northeast Passage in the Past Four
502   Decades. *Advances in Atmospheric Sciences*. https://doi.org/10.1007/s00376-022-2040-3

503   Mu, L., Losch, M., Yang, Q., Ricker, R., Losa, S. N., & Nerger, L. (2018). Arctic-Wide Sea Ice
504   Thickness Estimates From Combining Satellite Remote Sensing Data and a Dynamic Ice-
505   Ocean Model with Data Assimilation During the CryoSat-2 Period. *Journal of*
506   *Geophysical Research: Oceans, 123*(11), 7763-7780.
507   https://doi.org/10.1029/2018JC014316

508   Mu, L., Yang, Q., Losch, M., Losa, S. N., Ricker, R., Nerger, L., & Liang, X. (2018). Improving
509   sea ice thickness estimates by assimilating CryoSat-2 and SMOS sea ice thickness data
510   simultaneously. *Quarterly Journal of the Royal Meteorological Society, 144*(711), 529-
511   538. https://doi.org/10.1002/qj.3225

512   Nerger, L., & Hiller, W. (2013). Software for ensemble-based data assimilation systems—
513   Implementation strategies and scalability. *Computers & Geosciences, 55*, 110-118.
514   https://doi.org/10.1016/j.cageo.2012.03.026

515   Nerger, L., Janjić, T., Schröter, J., & Hiller, W. (2012). A Unification of Ensemble Square Root
516   Kalman Filters. *Monthly Weather Review, 140*(7), 2335-2345.
517   https://doi.org/10.1175/MWR-D-11-00102.1

Nguyen, A. T., Menemenlis, D., & Kwok, R. (2011). Arctic ice-ocean simulation with optimized model parameters: Approach and assessment. *Journal of Geophysical Research-Oceans, 116*. https://doi.org/10.1029/2010JC006573

Ourmières, Y., Brankart, J. M., Berline, L., Brasseur, P., & Verron, J. (2006). Incremental Analysis Update Implementation into a Sequential Ocean Data Assimilation System. *Journal of Atmospheric and Oceanic Technology, 23*(12), 1729-1744. https://doi.org/10.1175/JTECH1947.1

Park, Y. Y., Buizza, R., & Leutbecher, M. (2008). TIGGE: Preliminary results on comparing and combining ensembles. *Quarterly Journal of the Royal Meteorological Society, 134*(637), 2029-2050. https://doi.org/10.1002/qj.334

Parkinson, C. L., & Washington, W. M. (1979). A large-scale numerical model of sea ice. *Journal of Geophysical Research: Oceans, 84*(C1), 311-337. https://doi.org/10.1029/JC084iC01p00311

Petty, A. A., Kurtz, N. T., Kwok, R., Markus, T., & Neumann, T. A. (2020). Winter Arctic Sea Ice Thickness From ICESat-2 Freeboards. *Journal of Geophysical Research: Oceans, 125*(5), e2019JC015764. https://doi.org/10.1029/2019JC015764

Petty, A. A., Stroeve, J. C., Holland, P. R., Boisvert, L. N., Bliss, A. C., Kimura, N., & Meier, W. N. (2018). The Arctic sea ice cover of 2016: a year of record-low highs and higher-than-expected lows. *The Cryosphere, 12*(2), 433-452. https://doi.org/10.5194/tc-12-433-2018

Petty, A. A., Schröder, D., Stroeve, J. C., Markus, T., Miller, J., Kurtz, N. T., et al. (2017). Skillful spring forecasts of September Arctic sea ice extent using passive microwave sea ice observations. *Earth's Future, 5*(2), 254-263. https://doi.org/10.1002/2016EF000495

Pfaffling, A., Haas, C., & Reid, J. E. (2007). Direct helicopter EM - Sea-ice thickness inversion assessed with synthetic and field data. *Geophysics, 72*(4), F127-F137. https://doi.org/10.1190/1.2732551

Qi, D., Ouyang, Z., Chen, L., Wu, Y., Lei, R., Chen, B., et al. (2022). Climate change drives rapid decadal acidification in the Arctic Ocean from 1994 to 2020. *Science, 377*(6614), 1544-1550. https://doi.org/10.1126/science.abo0383

Rantanen, M., Karpechko, A. Y., Lipponen, A., Nordling, K., Hyvärinen, O., Ruosteenoja, K., et al. (2022). The Arctic has warmed nearly four times faster than the globe since 1979.

Communications Earth & Environment, 3(1), 168. https://doi.org/10.1038/s43247-022-00498-3

Ricker, R., Hendricks, S., Helm, V., Skourup, H., & Davidson, M. (2014). Sensitivity of CryoSat-2 Arctic sea-ice freeboard and thickness on radar-waveform interpretation. *The Cryosphere, 8*(4), 1607-1622. https://doi.org/10.5194/tc-8-1607-2014

Semtner, A. J. (1976). A Model for the Thermodynamic Growth of Sea Ice in Numerical Investigations of Climate. *Journal of Physical Oceanography, 6*(3), 379-389. https://doi.org/10.1175/1520-0485(1976)006<0379:AMFTTG>2.0.CO;2

Spreen, G., Kaleschke, L., & Heygster, G. (2008). Sea ice remote sensing using AMSR-E 89-GHz channels. *Journal of Geophysical Research: Oceans, 113*(C2). https://doi.org/10.1029/2005JC003384

Stroeve, J., Liston, G. E., Buzzard, S., Zhou, L., Mallett, R., Barrett, A., et al. (2020). A Lagrangian snow evolution system for sea ice applications (SnowModel-LG): Part II—Analyses. Journal of Geophysical Research: Oceans, 125, e2019JC015900. https://doi.org/10.1029/2019JC015900

Stroeve, J., & Notz, D. (2018). Changing state of Arctic sea ice across all seasons. *Environmental Research Letters, 13*(10), 103001. https://doi.org/10.1088/1748-9326/aade56

Tian-Kunze, X., Kaleschke, L., Maaß, N., Mäkynen, M., Serra, N., Drusch, M., & Krumpen, T. (2014). SMOS-derived thin sea ice thickness: algorithm baseline, product specifications and initial verification. *The Cryosphere, 8*(3), 997-1018. https://doi.org/10.5194/tc-8-997-2014

Xie, J., Counillon, F., & Bertino, L. (2018). Impact of assimilating a merged sea-ice thickness from CryoSat-2 and SMOS in the Arctic reanalysis. *The Cryosphere, 12*(11), 3671-3691. https://doi.org/10.5194/tc-12-3671-2018

Xiu, Y., Luo, H., Yang, Q., Tietsche, S., Day, J., & Chen, D. (2022). The Challenge of Arctic Sea Ice Thickness Prediction by ECMWF on Subseasonal Time Scales. *Geophysical Research Letters, 49*(8), e2021GL097476. https://doi.org/10.1029/2021GL097476

Yang, Q., Losa, S. N., Losch, M., Jung, T., & Nerger, L. (2015). The role of atmospheric uncertainty in Arctic summer sea ice data assimilation and prediction. *Quarterly Journal*

579   *of the Royal Meteorological Society, 141*(691), 2314-2323.
580   https://doi.org/10.1002/qj.2523

581 Yang, Q., Mu, L., Wu, X., Liu, J., Zheng, F., Zhang, J., & Li, C. (2019). Improving Arctic sea
582   ice seasonal outlook by ensemble prediction using an ice-ocean model. *Atmospheric*
583   *Research, 227*, 14-23. https://doi.org/10.1016/j.atmosres.2019.04.021

584 Yang, Q., Losa, S. N., Losch, M., Tian-Kunze, X., Nerger, L., Liu, J., et al. (2014). Assimilating
585   SMOS sea ice thickness into a coupled ice-ocean model using a local SEIK filter. *Journal*
586   *of Geophysical Research: Oceans, 119*(10), 6680-6692.
587   https://doi.org/10.1002/2014JC009963

588 Zhang, J., & Hibler, W. D. (1997). On an efficient numerical method for modeling sea ice
589   dynamics. *Journal of Geophysical Research: Oceans, 102*(C4), 8691-8702.
590   https://doi.org/10.1029/96JC03744

591 Zhou, X., Min, C., Yang, Y., Landy, J. C., Mu, L., & Yang, Q. (2021). Revisiting Trans-Arctic
592   Maritime Navigability in 2011–2016 from the Perspective of Sea Ice Thickness. *Remote*
593   *Sensing, 13*(14), 2766. https://doi.org/10.3390/rs13142766

594